Theor Chem Acc (2007) 117:1131–1143
DOI 10.1007/s00214-006-0222-1

REGULAR ARTICLE

Excited state dynamics with the direct trajectory surface hopping method: azobenzene and its derivatives as a case study

Giovanni Granucci · Maurizio Persico

Received: 30 August 2006 / Accepted: 13 October 2006 / Published online: 13 December 2006

Abstract We review the recent studies of the photoisomerization dynamics of azobenzene and its derivatives by surface hopping simulations based on semiempirical potential energy surfaces. We examine the ability of semiclassical methods to predict the excited state dynamics and to reproduce transient spectroscopic signals that constitute the most direct experimental evidence in this field. We show that the available simulation methods yield a deep insight into the mechanism of photochemical reactions and excited state decay, and a fairly good quantitative agreement with experimental findings. Probably the most important technical improvements we can envisage concern the surface hopping algorithm and the usage of ab initio data in the simulation of transient spectra. Concerning azobenzene, our results show that the isomerization mechanism is torsion of the N=N double bond, both by $n \rightarrow \pi^*$ and by $\pi \rightarrow \pi^*$ excitation. The influence of the solvent and the findings of some recent femtochemistry experiments deserve further work to be fully interpreted.

Keywords Azobenzene · Surface hopping · Semiclassical wavepacket dynamics · Photoisomerization · Nonadiabatic dynamics · Semiempirical calculations

1 Introduction

We have recently performed a set of computational simulations of the photoisomerization dynamics of azobenzene [1,2] and two of its derivatives [3,4] by means of a trajectory surface hopping (TSH) method, coupled with "on the fly" semiempirical electronic calculations. Some of the simulations were also carried out by the Full Multiple Spawning (FMS) method [2]. In this paper we review the results of those studies and put them in perspective, essentially with two aims: to offer a critical evaluation of the TSH method, with focus on the simulation of photoisomerizations and transient spectra, and to discuss the recent experimental and theoretical findings about azobenzene photochemistry.

First, we would like to set the approach we employed, i.e. trajectory surface hopping with semiempirical potential energy surfaces (PES), in the landscape of methods for excited state dynamics. To run such calculations, one has to select the theoretical level to treat both the electronic problem and the coupled nuclear-electronic dynamics. Moreover, one can choose to run the electronic structure calculations preliminarily or during the integration of the dynamics: the latter option, which is ours, is labeled as "direct" or "on the fly." We shall see that our choices yield a rather good quantitative agreement with experimental results and allow us to treat chromophore and reactive centers such as azobenzene, even when they interact with a much more extended chemical environment. Our basic technique of nonadiabatic trajectories, with on the fly semiempirical calculation of the electronic quantities, can be combined with practically any recipe for the semiclassical treatment of radiationless transitions and also with localized quantum wavepacket calculations [2,5]. While the reparameterized semiempirical PES seem to be adequate for most purposes, an integration with ab initio calculations may be necessary to improve the accuracy of the computed transient signals, generated by probe techniques such as

G. Granucci · M. Persico (✉)
Dipartimento di Chimica e Chimica Industriale,
Università di Pisa, v. Risorgimento 35, Pisa, 56126, Italy
e-mail: mau@dcci.unipi.it

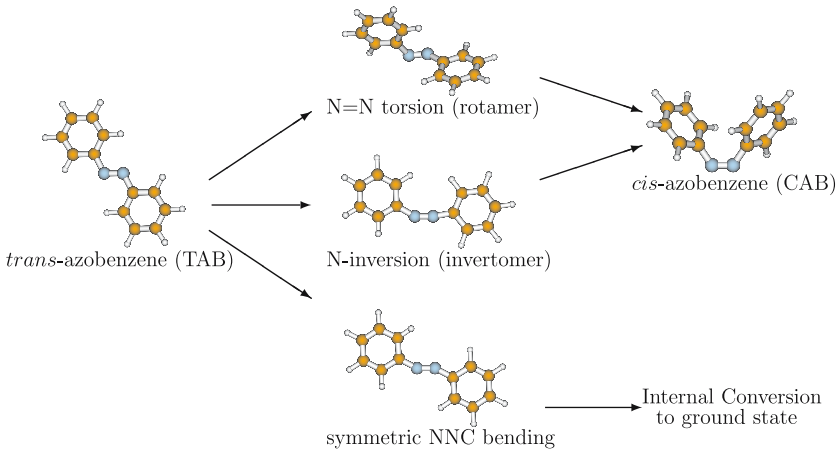

Fig. 1 Azobenzene photoisomerization and excited state decay pathways

up-converted fluorescence, differential absorption and especially for photoionization [6,7].

The photoisomerization mechanism of azobenzene (see Fig. 1) has been debated for many years. Two pathways, N=N double bond torsion and N inversion, were originally proposed for the isomerization, depending on whether the excitation wavelength fell into the $n \rightarrow \pi^*$ or $\pi \rightarrow \pi^*$ band [8–12]. Recently, at least one more internal coordinate, the symmetric NNC bending, has been suggested to be important in the decay of excited trans-azobenzene [13,14]. Our simulations [1] show that the torsional pathway is dominant in all cases (*cis* → *trans* or *trans* → *cis* photoisomerization, starting with $n \rightarrow \pi^*$ or $\pi \rightarrow \pi^*$ excitation). We found similar results for azobenzene derivatives in which the internal motions were somewhat hindered [3,4]. The accuracy of the simulations on azobenzene itself is confirmed by the good agreement with the measured photoisomerization quantum yields and with the sub-ps decay times obtained for the isolated molecule by time-resolved photoelectron spectroscopy (TRPES) [15]. However, most of the transient spectra were measured in solution [14,16–26], finding non-exponential decays with longer decay times (a few ps). Moreover, it is clear that the solvent viscosity has a strong influence on the decay of the fluorescence [14] and on the quantum yields [8,9,27–32]. We shall discuss the interpretation of such experiments and the feasibility of accurate simulations of the transient spectra by semiclassical methods.

2 Simulation methods

The choice of a simulation method for molecular dynamics can be reduced to three basic issues: one is how to treat the electronic problem (usually in a fixed nuclei adiabatic or diabatic representation), and the second is how to treat the nuclear dynamics, along with its coupling to the electronic dynamics if required by the physics of the process. The third issue is a very important technicality, namely, whether to solve the electronic problem beforehand or to do it "on the fly," during the integration of the dynamics.

Here, we shall focus on the nonadiabatic dynamics that characterizes most of the photochemical reactions. The need to take into account two or more electronic states, with (quasi) degeneracies and large geometrical distortions, restricts the choice of the computational approach to multiconfigurational or valence bond methods. The most frequently used ab initio technique is CASSCF and its variants, including perturbation corrections. Semiempirical MO and VB methods have also been used, in most cases with ad hoc parameterizations for single compounds or classes of compounds, since the standard parameter sets are only adequate for geometries close to the ground state equilibrium, and are not optimized for multiconfigurational treatments going beyond the single excitation CI.

The representation of the nuclear dynamics relies on a larger variety of methods (see for instance [33]). Fully quantum mechanical (QM) treatments, based on grid or static basis set representations of the nuclear wavepackets, can be applied to small molecules (less than 10 atoms) and for short propagation times (<1 ps). Computationally demanding processes, such as multiple pathway reactions, can limit even more severely the applicability of such methods. Probably the most powerful and versatile approach within this category is the multi-configurational time-dependent Hartree (MCTDH) method [34,35]. For instance, numerically exact MC-TDH calculations were recently performed on a model Hamiltonian with 21 nuclear coordinates, representing five electronic states of the pentatetraene cation, for a time interval of 120 fs [36].

The most drastic approximations that are usually introduced to avoid time and/or size limitations consist in assuming the validity of classical mechanics for the heavy particles or in reducing the dimensionality of the problem by considering only a few internal coordinates. The latter choice makes possible to treat larger systems, but is only valid for short times, because it ignores the energy transfer between different vibrational modes. The methods based on classical trajectories are appealing first of all because of being computationally viable also for large molecular systems and because the results of such simulations are easily analyzed to yield information about the reaction mechanisms and the nonadiabatic dynamics (see for instance [37–39] on the methods and [40] for recent applications in connection with control theory). We shall qualify these methods as semiclassical, since they mix classical mechanics for the nuclei and quantum mechanics for the electrons. This can be done in many different ways, due to the intrinsic arbitrariness of the semiclassical ansatz. Any new proposal in this field aims at reproducing more accurately the full QM dynamics, which implies avoiding some typical problems of internal consistency. In order to take into account both the QM uncertainty principle and the thermal distributions, one has to run many trajectories for each simulated experiment, with a suitable sampling of initial conditions.

A special status should be reserved for QM methods that make use of traveling basis functions to represent the nuclear wavepackets, as pioneered by Heller [41]. The FMS method [42] adapts a basis of traveling Gaussian functions to the needs of the nonadiabatic dynamics, reaching a very flexible compromise between the accuracy of the results and the computational effectiveness. For small systems and short times, it is possible to converge to almost exact results. When dealing with more exacting problems (many coordinates, long times), the accuracy is forcedly downgraded, but FMS still exhibits the basic features of a quantum mechanical treatment, at least concerning the nonadiabatic transitions (see [2,5,43] for recent applications). However, in these cases, FMS shares with the trajectory methods certain limitations, such as the need to perform several runs with different initial conditions, sampled by a stochastic algorithm: in fact, expanding the full vibrational wavepacket at $t = 0$ would require unmanageably large basis sets.

Whatever approaches are applied to solve the (static) electronic problem and to describe the nonadiabatic dynamics, these two steps can be performed separately. In this case, the PES and other electronic quantities (couplings, transition dipoles, etc.) are computed preliminarily and must be represented in a suitable analytic form. Decoupling the two problems has some advantages: this is the most convenient way to run very long simulations or to perform several computational experiments with different methods or initial conditions. However, when dealing with (near) degeneracy situations, such as conical intersections, finding analytical expressions for PES and couplings becomes a rather difficult task, usually solved by resorting to effective electronic Hamiltonians in a (quasi) diabatic representation [44,45]: a typical application is our treatment of azomethane photoisomerization and photodissociation [46,47]. For large molecules, a sufficiently complete sampling of the internal coordinate space with ab initio calculations can be totally unpractical, because the required number of single point calculations increases exponentially with the dimensionality of the problem. The alternative is offered by "direct" methods, whereby the electronic problem is solved "on the fly," i.e., during the integration of the dynamical equations. The direct approach is ideally suited for semiclassical dynamics, which only needs one electronic calculation for each time step, whereas the non-local character of quantum mechanics in principle would require the knowledge of the whole PES. However, the QM methods that make use of localized traveling basis functions, such as FMS, can also exploit the direct approach by introducing suitable approximations [2,5,42,43].

Direct dynamics can be computationally very demanding, since it requires $K \cdot N_S \cdot N_T$ electronic calculations, where N_S is the number of time steps and N_T is the number of trajectories. The factor K is 1 for semiclassical methods and $N_B \leq K \leq N_B(N_B + 1)$ in FMS, where N_B is the number of traveling basis functions. Ab initio direct dynamics for excited states has been pioneered by the research groups of Robb [48], Morokuma [49], Martínez [15,42], and others, and is nowadays quite a viable strategy with significant applications already demonstrated [50] and standard software available [51].

The search for computationally efficient alternatives has turned to semiempirical methods, either in VB [52] or MO–CI [53,54] schemes. The latter benefit from a long experience in the application to a large variety of compounds, mainly in the ground state but also in excited states, usually near the equilibrium geometry. In order to represent correctly bond breaking processes and orbital degeneracies, we introduced floating occupation numbers that depend on the MO energies (FOMO–SCF) and therefore on the molecular geometry [53]. The electronic wavefunctions are of CI type. Within this scheme, analytic energy gradients and nonadiabatic coupling matrix elements have been implemented by the Z-vector technique [3], put forward by Patchkovskii

and Thiel [55], whereby the cost of the coupled perturbed HF calculation is practically independent of the number of coordinates.

Large systems, where one can distinguish a chemically interesting core (chromophore and reacting center), embedded in a relatively inert environment, can be treated by QM/MM techniques. In our case [56,57], the core (QM) subsystem is treated at semiempirical level, and the environment by a standard Molecular Mechanics (MM) force field, such as AMBER [58] for biochemical matrices or the flexible SPC model [59] for water molecules. It is important to note that the electrostatic potential generated by the MM charges is included in the semiempirical Hamiltonian, so that the QM subsystem is polarized in a state-specific way, and the PES crossings are correctly displaced in geometry and energy [56]. The covalent bonding between QM and MM atoms is handled by an extension [3,57] of the "connection atom" approach of Antes and Thiel [60].

Our direct semiempirical or QM/MM approach to excited state dynamics has been implemented in the development versions of the MOPAC package [61]. It goes with a TSH dynamics [54], based on Tully's "fewest switches" algorithm [37,62], whose basic features and performance will be critically examined in the next section. Our implementation can be easily modified to accommodate other semiclassical models and has been coupled with the FMS method in collaboration with Martínez et al. in Urbana [2,5,43].

To conclude this section, we note that the boundary between direct and non-direct methods for the dynamics is not as clear-cut as it might to be thought. In fact, the preliminary work needed before starting a dynamical calculation cannot be completely avoided even with ab initio methods: some tests to choose basis sets and other options are normally performed. With semiempirical methods, one has to optimize at least partially a set of parameters, and this operation does not differ, in principle, from the determination of an effective Hamiltonian matrix with an arbitrary analytic expression. What makes the semiempirical approach preferable is its connection with an explicit form of the electronic wavefunctions, which determine the nonadiabatic couplings and other relevant matrix elements, and a certain degree of transferability of the optimized parameters. For instance, in the case of azobenzene [1], we made use of parameters already optimized for the benzene molecule and only readjusted those of the N atoms.

3 Azobenzene: photoisomerization mechanism and quantum yields

In this section, we compare the experimental and simulation results concerning the photodynamics of azobenzene. Historically, the first interesting clues about the photoisomerization mechanism of azobenzene were its quantum yields [8,9,27–32], obtained in different solvents by excitation into the first two absorption bands, $n \rightarrow \pi^*$ (S_1 state) and $\pi \rightarrow \pi^*$ ($S_2 - S_4$). Table 1 collects the quantum yields measured by many groups in different conditions, during about half a century of research (only some data concerning the $\pi \rightarrow \pi^*$ excitation of CAB, originally obtained by Bortolus and Monti [30] and later corrected by the same authors [32], have been discarded). Although the variety of sources does not warrant a perfect consistency of the data, two trends are quite well established: the *cis* $\rightarrow$ *trans* quantum yield

Table 1 Quantum yields for the azobenzene photoisomerization as functions of solvent polarity and viscosity, and simulation results

Exc. band	Polarity[a]	Viscosity[b]	$\Phi_{trans \rightarrow cis}$	$\Phi_{cis \rightarrow trans}$	Refs.
$\pi \rightarrow \pi^*$	Low	Low	0.09–0.13	0.40–0.44	[8,27–30,32]
	Medium	Low	0.12	0.40	[30,32]
	High	Low	0.16	0.35	[30,32]
	Protic	Low	0.10–0.22	0.30–0.50	[9,29–31]
	Low	High	0.05	0.40	[28]
	Protic	High	0.03–0.05	0.50	[28]
	TSH simulations, no solvent		0.15 ± 0.02	0.48 ± 0.03	[1]
$n \rightarrow \pi^*$	Low	Low	0.21–0.28	0.40–0.56	[8,27–30,32]
	Medium	Low	0.24–0.26	0.58–0.69	[30]
	High	Low	0.31	0.46	[30]
	Protic	Low	0.20–0.36	0.42–0.63	[9,29–31]
	Low	High	0.18	0.60	[28]
	Protic	High	0.23–0.42	0.53	[28]
	TSH simulations, no solvent		0.33 ± 0.03	0.61 ± 0.03	[1]
	FMS simulations, no solvent		0.46 ± 0.08	0.68 ± 0.11	[2]

[a] Solvent polarity: low, dielectric constant $\varepsilon < 4$; medium, $4 < \varepsilon < 10$; high, $\varepsilon > 10$, nonprotic solvent
[b] Solvent viscosity: low, $\eta < 3$ mPa·s; high, $\eta > 100$ mPa·s

$\Phi_{cis\rightarrow trans}$ is in all cases larger than the *trans* → *cis* one, $\Phi_{trans\rightarrow cis}$, and the quantum yields, especially $\Phi_{trans\rightarrow cis}$, are higher if one excites within the $n \rightarrow \pi^*$ band than within the $\pi \rightarrow \pi^*$ one. The former observation is easily explained by the relative stability of the two isomers, CAB being about 12 kcal/mol higher than TAB [63]: this difference reflects in the slopes of the excited state PES. The dependence of the quantum yield on the initial excited state is an obvious violation of Kasha's rule. No clear dependence on the wavelength, within each of the $n \rightarrow \pi^*$ and $\pi \rightarrow \pi^*$ bands, has been found [27,31]. For several years, the most popular explanation of these observations, originally put forward by Rau [8], was that in S_1 and in S_2 two different isomerization mechanisms would be active, namely N-inversion and N=N double bond torsion, respectively. This hypothesis was reinforced by the finding that supposedly "rotation-locked" azobenzene derivatives are able to isomerize, and actually their quantum yields for $\pi \rightarrow \pi^*$ excitation are enhanced with respect to azobenzene itself [8–10]. Also, the pioneering theoretical work of Monti et al. [64] with a minimal basis set supported this interpretation.

Later calculations [65–68] took into account more electronic states (at least two $\pi \rightarrow \pi^*$ states are needed for a correct interpretation of photochemistry) at better ab initio levels (CASSCF and MRCI with at least double-zeta basis sets). It was then shown that the inversion pathway is only viable in the $n \rightarrow \pi^*$ S_1 state, and the torsional one is energetically favored in both S_1 and S_2. A conical intersection between the S_0 and S_1 PES was located near the minimum of S_1, at the rotamer geometry (CNNC dihedral angle of about 95°). Moreover, Diau showed that a conical intersection between S_0 and S_1 can also be reached by a symmetric NNC bending motion, although at slightly higher energies [13]. Our semiempirical FOMO–SCF–CI calculations [1] were able to reproduce with good accuracy all these features, although some of the most recent theoretical results were not yet available when the reparameterization was performed (namely, those by Diau and Orlandi et al.). It was then possible to perform more thorough explorations of the PES, showing that the rotameric and the symmetric bending conical intersections belong to the same crossing seam, which can be reached from the Franck–Condon region by combining the two internal motions. Figure 2 is a polar plot showing the essential features of the S_1 PES and of its crossings with the two neighboring states, as a function of the CNNC and NNC angles.

It should be stressed that the sheer knowledge of the PES is not sufficient to prove that the torsional mechanism is quite dominant in the photoisomerization, nor what mixture of torsion and symmetric bending is most

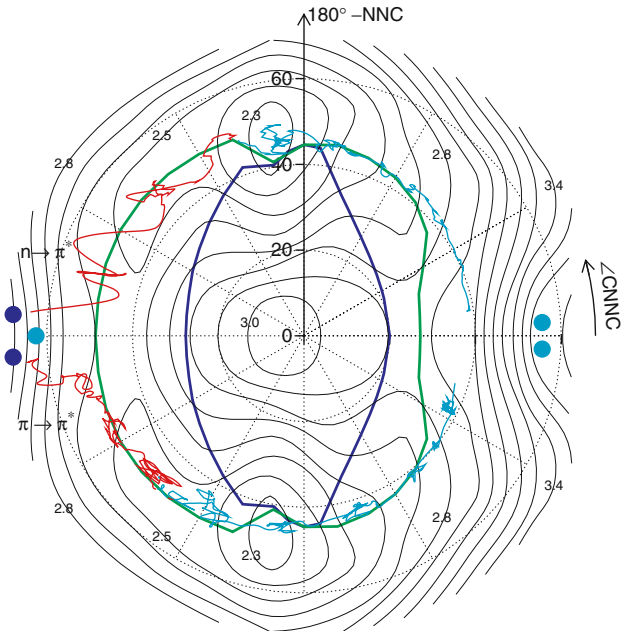

Fig. 2 S_1 potential energy surface of azobenzene by the semiempirical FOMO–SCF–CI method and average *trans* → *cis* trajectories. The radial coordinate in the polar plot is the complement to 180° of one NNC angle, and the angular coordinate is the CNNC dihedral. The distance between the contour lines is 0.1 eV and some lines are marked with energy values (eV) relative to the TAB equilibrium geometry in the ground state. Most of the plot shows the minimal energy PES of S_1 (all other coordinates, including the other NNC angle, having been optimized), but in the proximity of the Franck–Condon points the PES goes up to the vertical transition energy, for a more realistic picture of the photoprocess. The Franck–Condon points are marked by *light blue dots* (*trans* and *cis* isomers on the left and right hand sides, respectively). The *dark blue dots* mark the conical intersection between S_1 and S_2 and the *blue line* is the S_0–S_1 crossing seam. The *green line* is the minimum energy path along the torsional coordinate in S_1. Two average trajectories were obtained by averaging the CNNC and both NNC angles over all reactive trajectories (i.e., those starting from TAB and ending at CAB). The trajectories relative to $n \rightarrow \pi^*$ and to $\pi \rightarrow \pi^*$ excitation are shown in the *upper* and in the *lower half circles*, respectively. A *red line* is used until more than half of the individual trajectories run on one of the excited PES (S_1, most of the time), and a *light blue line* when most trajectories are in S_0

effective in the decay of the S_1 state. Even less could one explain why the $n \rightarrow \pi^*$ excitation leads to photoisomerization with a probability that is almost double than in the $\pi \rightarrow \pi^*$ case. The answers were sought by running simulations of photodynamics for the four cases: starting from the *cis* or *trans* isomers and with $n \rightarrow \pi^*$ or $\pi \rightarrow \pi^*$ excitation [1]. The TSH simulation results, obtained for an isolated molecule, are in rather good agreement with experiments (see Table 1): they are close to the upper end of the range of quantum yields obtained with nonpolar low-viscosity solvents.

The mechanism is essentially torsional in all four cases. Figures 2 and 3 show only the *trans* → *cis* conver-

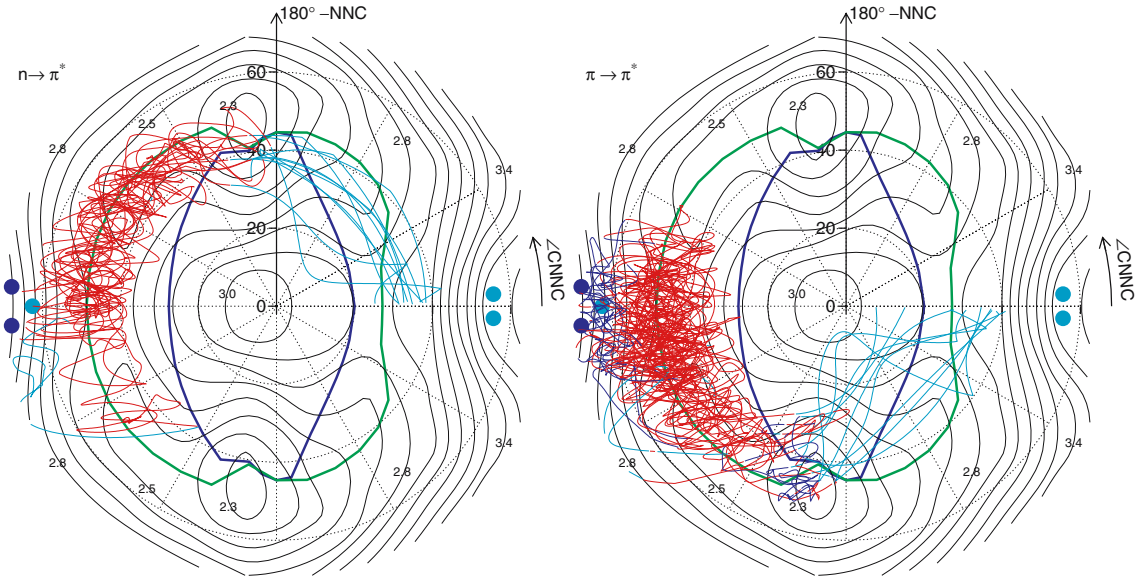

Fig. 3 Ten representative trajectories for the $n \rightarrow \pi^*$ and for the $\pi \rightarrow \pi^*$ excitation. Same polar plots as in Fig. 2, but individual trajectories are shown have been used instead of averages. The radial coordinate is here defined as the complement to 180° of the larger of the two NNC angles, in order to bring out trajectories that approach the inversion pathway. *Blue, red* and *light blue lines* are used for the portions of each trajectory running in $S_2 - S_3$, S_1, and S_0, respectively

sion. In Fig. 2 we have drawn two average trajectories, for $n \rightarrow \pi^*$ and $\pi \rightarrow \pi^*$ excitation: here the CNNC dihedral (angular coordinate in the polar plot) and both NNC angles (together) are averaged over all the reactive trajectories (i.e., those leading to isomerization). In Fig. 3 we show a set of ten representative trajectories for each of the two excitation bands, without averaging; in this case the larger of the two NNC angles is taken, at each time step, in order to bring out the N-inversion mechanism. The first figure shows that initially the NNC angles tend to open in the S_1 PES and then the trajectories follow the minimum energy path along the torsional coordinate. This is due to the difference in the NNC equilibrium values for the relevant electronic states: 117° in S_0 and 132° in S_1. By $n \rightarrow \pi^*$ excitation, the NNC symmetric bending coordinate oscillates in phase for all trajectories and such oscillations are well represented by the average trajectory: as a consequence, they should be experimentally detectable. In the case of $\pi \rightarrow \pi^*$ excitation, a fast decay to S_1 takes place ($\sim$0.1 ps), therefore each trajectory starts on the S_1 PES, close to the $S_1 - S_2$ conical intersection (NNC $\simeq$ 112°) with a different delay: the NNC oscillations then disappear in the average. However, in Fig. 3, we can see that the NNC angle undergoes even wider oscillations by $\pi \rightarrow \pi^*$ than by $n \rightarrow \pi^*$ excitation, because more energy is available and the starting point on the S_1 PES is located further from the NNC equilibrium value ($S_1 - S_2$ conical intersection versus Franck–Condon point). Therefore, the crossing seam between S_0 and S_1 is reached earlier by $\pi \rightarrow \pi^*$ excitation, with CNNC angles closer to the geometry of the initial isomer. As a result, the $\pi \rightarrow \pi^*$ quantum yields are lower than the $n \rightarrow \pi^*$ ones, although qualitatively the reaction mechanism is the same. It should be noted that the majority of trajectories hop to S_0 before reaching the midpoint along the torsional pathway, i.e., the top of the barrier in S_0, even when starting in S_1: in fact, the angular momentum gathered along the torsional coordinate before the nonadiabatic transition is another important factor that determines the quantun yields (see the statistical analysis in Ref. [1]). Figure 3 also shows that, once the molecule has reached the ground state with a large excess of vibrational energy, the pathway it follows is much less constrained and N-inversion becomes a viable option: in fact, many trajectories approach rather close to the linear N–N–C geometry (center of the polar plot). However, it should be reminded that a full inversional pathway would just be a straight line from left to right in the polar plot, whereas the computed trajectories follow the torsional pathway with symmetric NNC oscillations during the whole geometrical relaxation in S_1, which determines the quantum yield and takes a larger part of a isomerization time.

We obtained similar results [3] by simulating the *trans*, *trans* $\rightarrow$ *cis*, *trans* photoisomerization of 2,19-dithia [3.3](4,4′)-*trans*-diphenyldiazeno<2>phane (2S-ABP),

a compound with two stacked azobenzene moieties connected by $–CH_2–S–CH_2–$ bridges, experimentally studied by Rau and Lüddecke [8] and more recently by Diau et al. [69]. The distinctive feature of this system is that the quantum yields are equally high for both by $n \rightarrow \pi^*$ and $\pi \rightarrow \pi^*$ excitation. According to the simulation results, the steric constraints that distinguish 2S-ABP from azobenzene do not change substantially the isomerization mechanism: pure torsion prevails in the excited state, i.e., in the first half of the reaction pathway, and a mixture of torsion and inversion is observed after reversion to the ground state (compare Fig. 3 in this work with Fig. 6 in Ref. [3]). The stacking of the phenyl rings in 2S-ABP results in torsion of the N–C bonds, concerted with that of the N=N bond and such that both rings of the isomerizing azobenzene moiety remain as parallel as possible to those of the other one (a sort of double crank motion). The computed quantum yields for 2S-ABP excitation in the $n \rightarrow \pi^*$ and $\pi \rightarrow \pi^*$ bands were almost equal, as in the photoisomerization experiments, but much lower: about 0.07 instead of 0.21–0.24. This disagreement may be partly due to the fact that one of the two azobenzene moieties cannot isomerize, because it is treated by a ground state force-field in a QM/MM approach. Also, the torsional potential of the phenyl rings around the N–C bonds may be too rigid and hinder the crank motion. Finally, as we shall discuss below, the surface hopping method may overestimate the radiationless transition rates, so biassing the competition between excited state decay and isomerization.

The surface hopping simulations of the photoisomerization of azobenzene by $n \rightarrow \pi^*$ excitation were validated by comparison with FMS calculations using the same semiempirical PES [2] (see also Table 1). The FMS results confirmed that the quantum yields are determined by the competition between the nonadiabatic decay, which causes the reversion to the initial isomer if it occurs too early, and the forward motion along the torsional coordinate, leading to isomerization. According to FMS, the balance is slightly more favorable to the isomerization, so the quantum yields are higher than those obtained by TSH. Again, one may attribute this discrepancy to a bias of TSH towards faster excited state decay, apparently connected with a lack of internal consistency of the method. The fewest switches algorithm for surface hopping [37,62] was devised to distribute the trajectories among the electronic states according to the state probabilities, computed by solving the electronic time-dependent Schrödinger equation (TDSE). However, the actual state populations can differ from the computed probabilities for at least two reasons, which will be more closely investigated in a forthcoming paper [70]. One source of inconsistency is frequently referred to as the "frustrated hops" problem [71–73]. A frustrated hop occurs when the trajectory should jump from a lower to a higher PES, but the nuclear kinetic energy is smaller than the potential energy gap, so that the energy conservation cannot be enforced by reducing the nuclear momenta. In that case, the most usual option is to give up hopping, as we do in our simulations: this choice has been recently supported by theoretical considerations and numerical tests [73]. There is a less commonly recognized source of disagreement between state populations and computed probabilities. An assumption underlying the fewest switches algorithm is that the computed state probabilities are the same for all trajectories starting with the same initial conditions. In fact this is approximately true in some simple systems or models, for instance when an avoided crossing between excited states can be crossed only once as in direct photodissociations. On the contrary, the photoisomerization of a large polyatomic system normally goes through a strong interaction region, at or near a conical intersection, that is also close to the minimum of the excited state PES, as in the case of azobenzene. Then, till the system is in the excited state, it is attracted towards the interaction region and the transition probability tends to be high. After hopping to the ground state, instead, the trajectory runs downwards, towards regions where the ground to the excited state energy gap is larger and the transition probability much smaller. As a consequence, the computed state probabilities are very different functions of time for trajectories that have undergone a hop and for those that have not. A quantitative analysis [70] shows that the excited state populations, computed with the fewest switches algorithm, in such cases tend to be depleted faster than expected on the basis of the computed average probabilities, even discounting the effect of frustrated hops. One may thus suspect that the internal conversion times, as computed by surface hopping, tend to be too short.

4 Azobenzene: time-resolved spectroscopy

The most direct experimental information about the excited state and isomerization dynamics is gained through several techniques for detecting transient spectra: fluorescence [14,23], differential absorption [17–19], IR and Raman [20,22], and photoionization [15] have all been applied to azobenzene. It should be kept in mind that none of the transient signals is simply proportional to the excited state population, when the geometrical relaxation and the electronic state decay have similar time scales, so that their effects on the spectral properties do

mix. As a consequence, different detection techniques yield significantly different decay times. For instance, longer fluorescence wavelengths correspond to longer lifetimes, because the excited wavepacket moves in time towards lower regions of the excited PES, with smaller $S_0 - S_1$ energy gaps. The difference between the excited state populations, as computed by our simulations, and the experimental transients is well illustrated in the case of $n \rightarrow \pi^*$ excitation of TAB: the S_1 population remains very close to 1 during the first 150 fs [1], while all kinds of transients have been successfully fitted by one or two exponentials. The decay of the excited state is delayed because a rotation of the CNNC dihedral by about 70° is needed to reach the strong interaction region and start the hops (the same is found with FMS simulations [2]). It is thus necessary to simulate directly the experimental time-dependent spectra, in order to validate the computational results, and to relate the experimental data with the detailed description of the excited state dynamics: without establishing such a relationship, the interpretation of many interesting experiments would remain largely hypothetical.

Here we shall focus on the time-resolved fluorescence results, because they are more easily simulated than absorption or photoelectron spectra, as we shall discuss at the end of this section. In all cases, the relevant physical quantities are computed as averages over the N_T trajectories that have been run. In fluorescence simulations, the time-dependent total emission rate is defined as

$$F_{\mathrm{tot}}(t) = \frac{1}{N_T} \sum_{i=1}^{N_T} \sum_{K=0}^{L_i - 1} A_{L_i \rightarrow K}, \tag{1}$$

where i numbers the single trajectory, L_i is the current electronic state at time t for the i-th trajectory, and $A_{L_i \rightarrow K}$ is the Einstein coefficient for the transition to a state K lower than L_i:

$$A_{L \rightarrow K} = \frac{4(E_L - E_K)^3 \mu_{LK}^2}{3\hbar^4 c^3}. \tag{2}$$

Besides the current state index L_i, the electronic energy differences $E_L - E_K$ and the transition dipoles μ_{LK} too depend on time through the molecular geometry. The time-dependent fluorescence spectrum $F(\lambda, t)$ is obtained in the same way, but selecting the transitions with $E_L - E_K = hc/\lambda$, within a certain tolerance ΔE:

$$F(\lambda, t) = \frac{1}{2N_T \Delta E} \sum_{i=1}^{N_T} \sum_{K=0}^{L_i - 1} A_{L_i \rightarrow K} f(E_L - E_K, \lambda). \tag{3}$$

Here the factor f is 1 for $|E_L - E_K - hc/\lambda| \leq \Delta E$ and is 0 otherwise. The steady-state spectrum and the fluorescence quantum yield are obtained as time-integrated quantities:

$$F(\lambda) = \int_0^\infty F(\lambda, t) \mathrm{d}t \tag{4}$$

$$\Phi_f = \int_0^\infty F_{\mathrm{tot}}(t) \mathrm{d}t. \tag{5}$$

In practice, the integrals are replaced by summations over the time steps at which we calculate the transition dipoles. For the quantum yield, we also add a small correction for times beyond the stopping time of all trajectories ($t_{\max} = 1$ ps), computed on the basis of an exponential fit of F_{tot}.

By $\pi \rightarrow \pi^*$ excitation of TAB in hexane, Fujino et al. [23] observed two fluorescence bands, peaked at ~390 and 6–700 nm, that were easily assigned to the $S_2 \rightarrow S_0$ and $S_1 \rightarrow S_0$ transitions, respectively. They evaluated the emission quantum yields Φ_f for each band on the basis of the measured lifetimes and absorption oscillator strengths, and obtained 2.5×10^{-5} for the $\pi \rightarrow \pi^*$ band and 7.5×10^{-7} for the $n \rightarrow \pi^*$ one. In Fig. 4 we show the computed steady-state spectrum, which is very similar to the experimental one [23]. In the same figure, we also show the contributions of emission from the $\pi \rightarrow \pi^*$ states (S_2 and S_3, grouped together), and from the $n \rightarrow \pi^*$ one, S_1. The latter presents a maximum, in coincidence with the long wavelength queue of the $\pi \rightarrow \pi^*$ band, which could not be separated from it by the analysis of the experimental data. In fact,

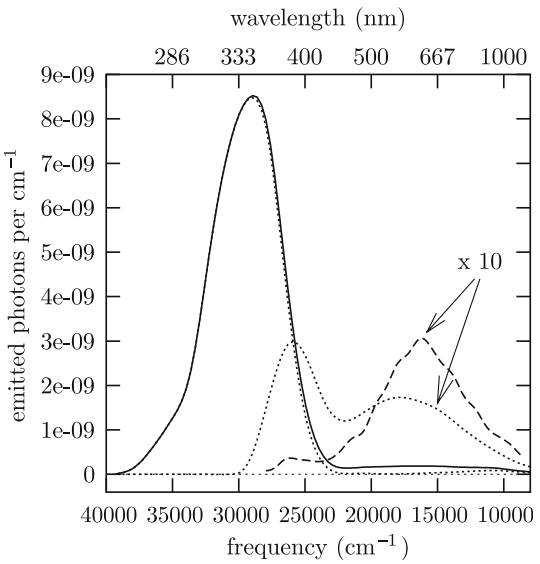

Fig. 4 Simulated steady-state fluorescence spectra of TAB: *full lines* $\pi \rightarrow \pi^*$ excitation; *dashed lines*, $n \rightarrow \pi^*$ excitation; *dotted lines*, $\pi \rightarrow \pi^*$ excitation, contributions from the S_2 and S_3 states (together) and from S_1

this is a short lifetime feature produced just after the $S_2 \rightarrow S_1$ surface hopping in the neighborhood of the $S_2 - S_1$ conical intersection: given the quasi-degeneracy of the PES and the mixing of the electronic wavefunctions, it would be difficult to distinguish the emission of the two states. On the other hand, because of the breakdown of the Born–Oppenheimer approximation, in such situations one should not attach too much significance to the adiabatic state labeling. Therefore, we have separated the computed emission bands just on the basis of wavelength, setting the boundary at 480 nm. In this way, the computed quantum yields were $\Phi_f = 5.9 \times 10^{-5}$ for the $\pi \rightarrow \pi^*$ band and 2.3×10^{-6} for the $n \rightarrow \pi^*$ one. Since our simulations are based on transition dipole moments computed semiempirically, without taking care of such quantities in the parameterization, we may be satisfied with reproducing the experimental results within an order of magnitude. However, it should be noted that also the experimental estimates of the quantum yields, based on the oscillator strengths for absorption, are grossly approximated: given the fast geometrical relaxation that follows excitation, there is no reason to expect a close relationship between the emission and the absorption bands. This is especially true for the $n \rightarrow \pi^*$ transition, which is symmetry forbidden at the C_{2h} equilibrium geometry of TAB: the transition dipole for emission at strongly distorted geometries can be substantially larger than that for the absorption, which depends on the amplitude of the ground state vibrational motions. In fact, the ratio of the areas of the $\pi \rightarrow \pi^*$ and $n \rightarrow \pi^*$ emission bands, shown in Fig. 3 of Ref. [23], is about 20, while that between the estimated quantum yields is about 30. For the computed quantum yields, we find a ratio of 25.

We fitted the decay of the $\pi \rightarrow \pi^*$ fluorescence ($\lambda <$ 480 nm) by a linear combination of two independent exponentials: we obtained a lifetime $\tau_1 = 94$ fs for the main component, and a minor component (7%) with $\tau_2 = 524$ fs, in good agreement with the experimental finding (110 fs). For the $n \rightarrow \pi^*$ fluorescence ($\lambda >$ 480 nm) we applied the consecutive decay law $F(t) \propto \exp(-t/\tau_2) - exp(-t/\tau_1)$ and obtained $\tau_1 = 79$ fs and $\tau_2 = 416$ fs (again in agreement with the experimental value of 500 fs). The time-dependent emission rates and state populations are shown in Fig. 5. We note that the ratio between the long wavelength emission and the S_1 population increases in time, because of the dependence of the $S_0 - S_1$ transition dipole on the CNNC twisting and other geometrical distorsions.

By $n \rightarrow \pi^*$ excitation of TAB in DMSO, Satzger et al. [25] registered the fluorescence spectrum and obtained $\Phi_f = 3.2 \times 10^{-6}$, again on the basis of the measured lifetimes and of the absorption spectrum. The

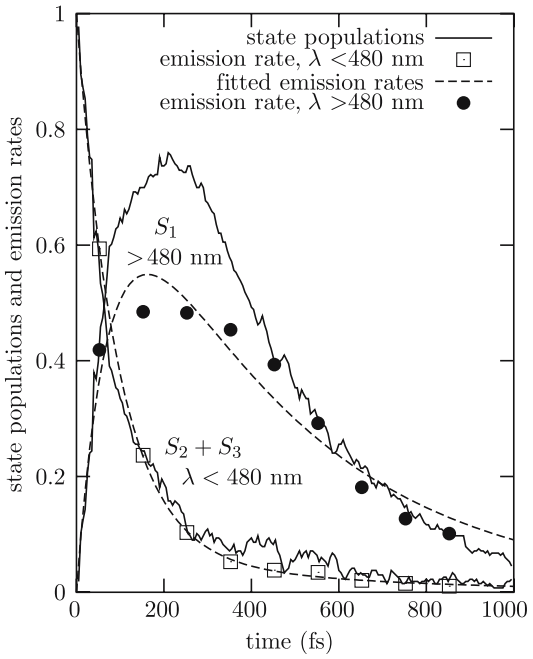

Fig. 5 Simulated decay of fluorescence and state populations, with $\pi \rightarrow \pi^*$ excitation. The emission rates are normalized in order to be comparable with the populations

simulated spectrum, shown in Fig. 4, agrees very well with the experimental one, and so does the computed quantum yield, $\Phi_f = 2.7 \times 10^{-6}$. We note that the computed Φ_f for emission with $\lambda > 480$ nm is only slightly smaller by $\pi \rightarrow \pi^*$ than by $n \rightarrow \pi^*$ excitation, while the influence of the excitation wavelength on the photoisomerization quantum yields is much more pronounced. This can be understood, considering that the emission takes place during all the time spent by the wavepacket on the S_1 PES at geometries where the $S_0 - S_1$ gap is still rather large, whereas the photoisomerization occurs if the internal coordinates and nuclear momenta are favorable at the time of the $S_1 \rightarrow S_0$ transition. Now, the kind of excitation affects more the geometry at which the molecule hits the $S_0 - S_1$ crossing seam (torsion versus symmetric bending) than the S_1 lifetime. We note that the experimental estimates of Φ_f given by Fujino et al. [23] for the $\pi \rightarrow \pi^*$ excitation and by Satzger et al. [25] for the $n \rightarrow \pi^*$ one differ by a factor ~4, which may be due to other differences in the experimental conditions and/or in the data analysis.

Almost all emission or absorption transients of azobenzene in various solvents were adequately fitted by two- or three-exponential laws [14,16–26]. For instance, for TAB in DMSO, Satzger et al. [25] found two main components with $\tau_1 = 0.34$ ps and $\tau_2 = 3.0$ ps. Our computed time-dependent fluorescence can be fitted by a single exponential with $\tau = 0.26$ ps (see Fig. 6). Diau

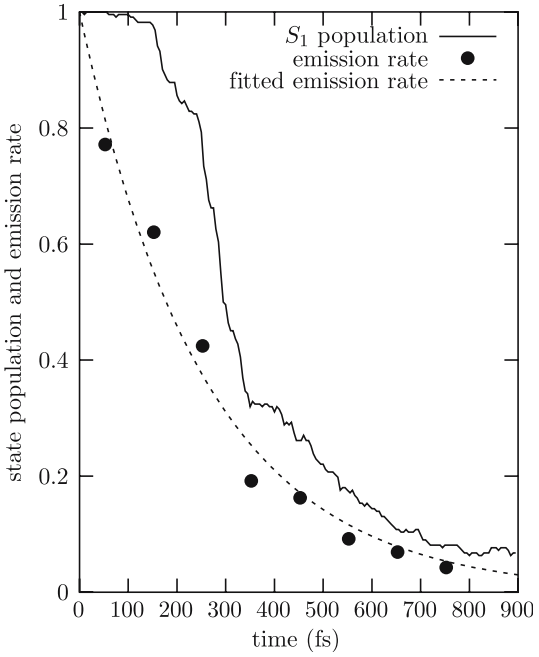

Fig. 6 Simulated decay of fluorescence and S_1 state population with $n \rightarrow \pi^*$ excitation. The emission rate is normalized in order to be comparable with the state population

et al. examined the dependence of the lifetimes on the emission wavelength [24] and on the solvent viscosity [14]. They fitted the fluorescence transients by a consecutive decay law in order to represent schematically a two-step mechanism taking place in the S_1 surface. With hexane as a solvent, they obtained τ_1 ranging from 160 to 275 fs in the interval of wavelengths 550–732 nm, while τ_2 goes from 0.78 to 1.56 ps. By considering spectral intervals of 100 nm centered at $\lambda = 500, 600$, and 700 nm, we obtain lifetimes of 175, 249, and 275 fs, respectively. As already observed, the λ dependence of the lifetimes is easily interpreted: in fact, longer wavelengths are emitted later, when the wavepacket reaches lower regions in the S_1 PES. Overall, our results agree with the short-time components of Refs. [24,25], but we miss the long-time component. This is probably due to the effect of the solvent that may hinder the large amplitude motions, in particular the CNNC torsion, needed to reach the funnel. Of course, the specific drawbacks of TSH and any inaccuracy of the PES may also play a role.

The nature of the solvent affects both the photoisomerization quantum yields (see Table 1) and the lifetimes [14]. Diau et al. compared the decay of TAB fluorescence by $n \rightarrow \pi^*$ excitation in hexane and in ethylene glycol. They also measured the time-dependent fluorescence anisotropy $r(t)$, and distinguished a fast component, characterized by an anisotropy parameter that is close to the theoretical maximum ($r = 0.4$) and constant in time, and a slow component. One lifetime τ_{slow} fits the decay of both intensity and anisotropy for the slow component: $F(t) = F(0)\exp(-t/\tau_{\text{slow}})$ and $r(t) = (r_0 - r_\infty)\exp(-t/\tau_{\text{slow}}) + r_\infty$. In hexane, the fast lifetime τ_{fast} goes from 120 to 330 fs, depending on the excitation and fluorescence wavelengths, and τ_{slow} goes from 0.6 to 2.0 ps. In the more viscous solvent, the fast component is biexponential and all the times are much longer: $\tau_{\text{fast},1} = 0.35 - 0.65$ ps, $\tau_{\text{fast},2} = 3.1 - 3.6$ ps, $\tau_{\text{slow}} = 20 - 24$ ps. The weight of the slow component, quite substantial in hexane solution (24–49%), is only 3% in ethylene glycol: apparently the high viscosity almost suppresses the decay of the fluorescence anisotropy, i.e., it prevents the reorientation of the transition dipole before emission. The authors interpreted these findings by assuming that two distinct pathways contribute to the excited state decay: the first mechanism is fast, does not change the orientation of the transition dipole and is moderately affected by the solvent viscosity; while the other one is slower, leads to fluorescence depolarization and is strongly inhibited by viscous solvents. The two mechanisms were tentatively identified with double symmetric inversion and with torsion, respectively. We plan to run simulations of azobenzene in different solvents, by the QM/MM variant of our method, to investigate the influence of solute–solvent interactions on the excited state dynamics, quantum yields, lifetimes and fluorescence depolarization. As to the last issue, any attempt to provide a theoretical interpretation requires the determination of the direction of the transition dipole for the $n \rightarrow \pi^*$ absorption, which is symmetry forbidden in TAB. An ab initio study currently in progress [74] has shown that the most effective internal coordinates in making the transition vibronically allowed are the torsions of the phenyl groups around the N–C bonds and, to a lesser extent, the CNNC torsion. The transition dipole lies in the CNNC plane and makes an angle of about 45° with the N–N axis. By increasing the CNNC torsion, the dipole tends to align with the N–N axis, so the identification of this coordinate as responsible for the depolarization is plausible.

The role of solvents in slowing down the internal conversion is indirectly confirmed by the TPRES experiment of Schultz et al. [15], showing no longtime components in the decay of an isolated molecule. By using an excitation wavelength of 330 nm ($\pi \rightarrow \pi^*$ band), the authors found two TRPES signals. The first one decays with a lifetime of 420 fs and its energy corresponds to the $S_3/S_4 \rightarrow D_2/D_3$ transitions (from two almost degenerate states of TAB to the second and third excited states of the TAB^+ ion), but also to $S_1 \rightarrow D_0$. The former assignment was preferred by Schultz et al. because they did not detect any delay in the appearance of the TRPES

band, and the S_3/S_4 states can be directly populated by 330 nm light absorption. However, the relatively long lifetime and the coincidence of the transition energies supports a partially different interpretation, namely that also the $S_1 \rightarrow D_0$ transition contributes to this signal. The second TRPES signal has a lifetime of 170 fs and is energetically compatible with the $S_2 \rightarrow D_0$ transition, which appears to be the most likely assignment.

Simulation of TRPES for large molecules is quite a demanding task [75]. The most important ingredient is the photoabsorption cross section σ for the relevant bound-free electronic transitions, which involve the excited states of the neutral molecule and possibly more than one electronic state of the ion. Also, one needs to evaluate the ionization quantum yields, Φ_i. Both quantities, σ and Φ_i, are functions of the molecular geometry and of the photon energy: they depend sharply on the excess energy, i.e., the kinetic energy of the outgoing electron, $E_T = h\nu - \Delta E$, where ΔE is the energy difference between the ion state and the neutral one. The photoabsorption cross sections can be computed by ab initio methods, but it would be computationally inconvenient to do it every few time steps for many trajectories. Valuable results can be obtained by assuming that σ and Φ_i are step functions, vanishing for $\Delta E < 0$ and constant for $\Delta E > 0$ [6,76]. However, considerable improvements with respect to this oversimplified model can be achieved by resorting to a mixed semiempirical/ab initio treatment [7]. With a suitable reparameterization, the ion energies and therefore the excess energy E_T can be computed at semiempirical level for a very large number of time steps. The knowledge of σ and Φ_i as functions of E_T and of the most important internal coordinates, based on a limited number of ab initio calculations and on empirical information, allows one to simulate the TPRES experiments. By computing also the anisotropy parameters of the outgoing electron, one would also access the time-resolved photoelectron angular distributions, a kind of experimental information that can provide valuable insight on the excited state dynamics, especially for partially aligned molecular samples [75,77].

The absorption spectra are more easily computed than the photoelectron ones. Still, one needs a sufficiently complete determination of higher energy electronic states that do not have part in the dynamics. Moreover, an important contribution to absorption comes from the hot ground state molecules, so an accurate simulation would require extensive knowledge of the transition dipoles as functions of the internal coordinates that may undergo large amplitude motions. This is well illustrated by our simulations of the *cis* $\rightarrow$ *trans* photoisomerization of a supramolecular system composed of an azobenzene chromophore connected with two cyclooctapeptides. Vollmer et al. [78] have shown that this compound can exist in two isomeric forms: *cis*, with the two peptide rings coupled by eight hydrogen bonds, and *trans*, whereby the two rings are disconnected (see also the computational study of Qu et al. [79]). The two isomers have quite different self-assembling properties and can be photoconverted into each other using light of the appropriate wavelengths. We took this as an example, among many other photoswitchable supramolecular systems (see Ref. [80] for a recent review), to study how the photoisomerization is hindered by specific interactions not directly affecting the chromophore. We found that the *cis* $\rightarrow$ *trans* conversion occurs in a very short time ($\sim$0.2 ps) and with a high quantum yield (0.59), as in azobenzene itself. However, immediately after the isomerization, the peptide rings remain coupled, and the azobenzene moiety is strongly distorted with respect to the free *trans* geometry. The hydrogen bonds start to break, with the assistance of the neighboring water molecules, in a much longer time scale (the process is far from complete after 1.5 ps). During this time, the azobenzene chromophore, now in the ground electronic state, transfers the excess vibrational energy to the environment and slowly approaches its equilibrium geometry. Our preliminary simulations of the transient absorption spectrum indicate that the hot ground state rearrangement process could be easily monitored experimentally, because the $n \rightarrow \pi^*$ band at distorted geometries is much stronger than at equilibrium.

5 Concluding remarks

In this paper we have considered the photoisomerization of azobenzene as a case study, and we have shown that a convincing description and explanation of the excited state dynamics can only be obtained by combining all the information gained by classical photochemistry and femtochemistry experimental techniques, by ab initio calculations and by computer simulations of the excited state dynamics. Using state-of-the-art technology, the simulations can be carried out by trajectory surface hopping techniques or, with a substantially heavier computational effort, by the FMS method. In both cases, the direct strategy allows one to run the dynamics with all the nuclear degrees of freedom, so circumventing the very cumbersome task of preparing analytic PES and coupling functions. Simulations performed with ab initio direct methods for a molecule of this size are feasible [15], but they are subject to severe limitations in practice, because of their computational burden. Resorting to semiempirical methods, in combination with Molec-

ular Mechanics to represent the chemical environment, seems to be nowadays the best compromise. The semiclassical/semiempirical approach has been able to represent correctly the mechanism and quantum yields of the photoisomerization of azobenzene in various circumstances [1–4]. Improvements of both the surface hopping algorithms and of the semiempirical PES can be envisaged and may be necessary in order to obtain a more accurate simulation of time-dependent experimental spectra. This is an important goal, both to validate the results of the simulated dynamics, and to reach a full understanding of the experimental results. For reasons depending mainly on the kind of electronic transitions involved, the fluorescence spectra are the most easily reproduced, even at semiempirical level. A satisfactory study of fluorescence depolarization, differential absorption or photoelectron spectroscopy will require the use of information derived from ab initio calculations, as already demonstrated on smaller systems [7].

Acknowledgments This work was supported by grants of the italian M.I.U.R. and of the University of Pisa.

References

1. Ciminelli C, Granucci G, Persico M (2004) Chem Eur J 10:2327
2. Toniolo A, Ciminelli C, Persico M, Martínez TJ (2005) J Chem Phys 123:234308
3. Ciminelli C, Granucci G, Persico M (2005) J Chem Phys 123:174317
4. Ciminelli C, Granucci G, Persico M in preparation
5. Toniolo A, Thompson AL, Martínez TJ (2004) Chem Phys 304:133
6. Barbatti M, Granucci G, Persico M, Lischka H (2005) Chem Phys Lett 401:276
7. Cacelli I, Evangelista F, Granucci G, Persico M, unpublished results
8. Rau H, Lüddecke E (1982) J Am Chem Soc 104:1616
9. Rau H (1984) J Photochem 26:221
10. Rau H, Yu-Quan S (1988) J Photochem Photobiol A 42:321
11. Rau H (1990) In: Durr H, Bouas-Laurent H, (eds) Photochromism. Molecules and systems Elsevier, Amsterdam, Chapt. 4, p 165
12. Horspool W (2000) In: Patai S (ed), The Chemistry of the hydrazo, azo and azoxy groups, vol 2, Wiley, New York
13. Diau EW-G (2004) J Phys Chem A 108:950
14. Chang C-W, Lu Y-C, Wang T-T, Diau EW-G (2004) J Am Chem Soc 126:10109
15. Schultz T, Quenneville J, Levine B, Toniolo A, Martínez TJ, Lochbrunner S, Schmitt M, Schaffer JP, Zgierski MZ, Stolow A (2003) J Am Chem Soc.125:8098
16. Tamai N, Miyasaka H (2000) Chem Rev 100:1875
17. Lednev IK, Ye T-Q, Hester RE, Moore JN (1996) J Phys Chem 100:13338
18. Lednev IK, Ye T-Q, Matousek P, Towrie M, Foggi P, Neuwahl FVR, Umapathy S, Hester RE, Moore JN (1998) Chem Phys Lett 290:68
19. Nägele T, Hoche R, Zinth W, Wachtveitl J (1997) Chem Phys Lett 272:489
20. Hamm P, Ohline SM, Zinth W (1997) J Chem Phys 106:519
21. Terazima M, Takezaki M, Yamaguchi S, Hirota N (1998) J Chem Phys 109:603
22. Fujino T, Tahara T (2000) J Phys Chem A 104:4203
23. Fujino T, Arzhantsev SYu, Tahara T (2001) J Phys Chem A 105:8123
24. Lu Y-C, Chang C-W, Diau EW-G (2002) J Chin Chem Soc 49:693
25. Satzger H, Spörlein S, Root C, Wachtveitl J, Zinth W, Gilch P (2003) Chem Phys Lett 372:216
26. Satzger H, Root C, Braun M (2004) J Phys Chem A 108:6265
27. Zimmermann G, Chow L-Y, Paik U-J (1958) J Am Chem Soc 80:3528
28. Gegiou D, Muszkat KA, Fischer E (1968) J Am Chem Soc 90:12
29. Ronayette J, Arnaud R, Lebourgeois P, Lemaire J (1974) Can J Chem 52:1848
30. Bortolus P, Monti S (1979) J Phys Chem 83:648
31. Gauglitz G, Hubig S (1985) J Photochem 30:121
32. Siampiringue N, Guyot G, Monti S, Bortolus P (1987) J Photochem 37:185
33. Jungwirth P, Gerber RB (1999) Chem Rev 99:1583
34. Beck MH, Jäckle A, Worth GA, Meyer H-D (2000) Phys Rep 324:1
35. Meyer H-D, Worth GA (2003) Theor Chem Acc 109:251
36. Markmann A, Worth GA, Mahapatra S, Meyer H-D, Köppel H, Cederbaum LS (2005) J Chem Phys 123:204310
37. Tully JC (1998) Faraday Discuss 110:407
38. Topaler MS, Allison TC, Schwenke DW, Truhlar DG (1998) J Chem Phys 109:3321
39. Drukker K (1999) J Comput Phys 153:225
40. Bonačić-Koutecký V, Mitrić R (2005) Chem Rev 105:11
41. Heller EJ (1975) J Chem Phys 62:1544
42. Ben-Nun M, Quenneville J, Martínez TJ (2000) J Phys Chem A 104:5161
43. Toniolo A, Olsen S, Manohar L, Martínez TJ (2004) Faraday Discuss. 127:149
44. Pacher T, Cederbaum LS, Köppel H (1993) Adv Chem Phys 84:293
45. Persico M (1998) In: Electronic diabatic states: definition, computation and applications. in Encyclopedia of Computational Chemistry; Schleyer PvR, Allinger NL, Clark T, Gasteiger J, Kollman PA, Schaefer III HF, Schreiner PR (Eds) Wiley, Chichester, p 852
46. Cattaneo P, Persico M (2000) Theoret Chem Acc 103:390
47. Cattaneo P, Persico M (2001) J Am Chem Soc 123:7638
48. Vreven T, Bernardi F, Garavelli M, Olivucci M, Robb MA, Schlegel HB (1997) J Am Chem Soc 119:12687
49. Kaledin AL, Morokuma K (2000) J Chem Phys 113:5750
50. Barbatti M, Aquino AJA, Lischka H (2006) Mol Phys 104:1053
51. Barbatti M, Granucci G, Lisckha H, Ruckenbauer M (2006) NEWTON-X, Institute of Theoretical Chemistry, University of Vienna
52. Clifford S, Bearpark MJ, Bernardi F, Olivucci M, Robb MA, Smith BR (1995) J Am Chem Soc 242:27
53. Granucci G, Toniolo A (2000) Chem Phys Lett 325:79
54. Granucci G, Persico M, Toniolo A (2001) J Chem Phys 114:10608
55. Patchkovskii S, Thiel W (1997) Theoret Chem Acc 98:1
56. Persico M, Granucci G, Inglese S, Laino T, Toniolo A (2003) J Mol Struct Theochem 621:119
57. Toniolo A, Ciminelli C, Granucci G, Laino T, Persico M (2004) Theoret Chem Acc 93:270

58. Case DA, Pearlman DA, Caldwell JW, T.E. Cheatham III Wang J, Ross WS, Simmerling CL, Darden TA, Merz KM, Stanton RV, Cheng AL, Vincent JJ, Crowley M, Tsui V, Gohlke H, Radmer RJ, Duan Y, Pitera J, Massova I, Seibel GL, Singh UC, Weiner PK, Kollman PA (2002) AMBER 7, University of California, San Francisco
59. Dang LX, Pettitt BM (1987) J Phys Chem 91:3349
60. Antes I, Thiel W (1999) J Phys Chem A 103:9290
61. Stewart JJP (2002) MOPAC 2000 and MOPAC 2002. Fujitsu Limited, Tokio, Japan
62. Tully JC (1990) J Chem Phys 93:1061
63. Adamson AW, Vogler A, Kunkely H, Wachter R (1978) J Am Chem Soc 100:1298
64. Monti S, Orlandi G, Palmieri P (1982) Chem Phys 71:87
65. Cattaneo P, Persico M (1999) PCCP 1:4739
66. Ishikawa T, Noro T, Shoda T (2001) J Chem Phys 115:7503
67. Gagliardi L, Orlandi G, Bernardi F, Cembran A, Garavelli M (2004) Theoret Chem Acc 111:363
68. Cembran A, Bernardi F, Garavelli M, Gagliardi L, Orlandi G (2004) J Am Chem Soc 126:3234
69. Lu Y-C, Diau EW-G, Rau H (2005) J Phys Chem A 109:2090
70. Granucci G, Persico M in preparation
71. Müller U, Stock G (1997) J Chem Phys 107:6230
72. Jasper AW, Truhlar DG (2003) Chem Phys Lett 369:60
73. Parandekar PV, Tully JC (2005) J Chem Phys 122:094102
74. Cusati T, Granucci G, Persico M, Spighi G in preparation
75. Seideman T (2002) Annu Rev Phys Chem 53:41
76. Mitrić R, Bonačić-Koutecký V, Pittner J, Lischka H (2006) J Chem Phys 125:024303
77. Suzuki Y, Stener M, Seideman T (2003) J Chem Phys 118:4432
78. Vollmer MS, Clark TD, Steinem C, Reza Ghadiri M (1999) Angew Chem Int Ed 38:1598
79. Qu W, Tan H, Chen G, Liu R (2003) Phys Chem Chem Phys 5:2327
80. Yager KG, Barrett CJ (2006) J Photochem Photobiol A 182:250